International Journal of Rock Mechanics and Mining Sciences 99 (2017) 21–27

Contents lists available at ScienceDirect

International Journal of Rock Mechanics and Mining Sciences

journal homepage: www.elsevier.com/locate/ijrmms

Evaluation of flexural failure of sill mats using classical beam theory and numerical models

Cristian Caceres[a,*], Ricardo Moffat[a], Rimas Pakalnis[b]

[a] Facultad de Ingenieria y Ciencias, Universidad Adolfo Ibáñez, Santiago, Chile
[b] Dept. of Mining Engineering, University of British Columbia, Vancouver, Canada

ARTICLE INFO

Keywords:
Sill mat
Numerical model
Mining
Flexural failure

1. Introduction

Sill mats are structural elements that provide support in underground mining (Fig. 1). In vertical or sub-vertical orebodies, an ore sill pillar is replaced by a sill mat counterpart when the economic benefit is positive, such as when the ore grade is enough to make positive earnings. A sill mat is constructed using multiple batches of cemented rock fill or pastefill (cemented tailings) placed into the previously mined ore sill pillar to a predefined height derived from its design. Sill mats may or not be anchored to the hanging and foot walls, and usually are sufficiently long in the longitudinal direction making a two-dimensional analysis appropriate to be performed. When the underlying stope is removed, the load of the unconsolidated backfill that rests on top of the sill mat and its self-weight must be supported by this structural element. Therefore, a correctly designed sill mat should be stable under these loads, allowing the safe operation of mining personnel and equipment underneath it. The proper design of these mining structures requires the correct determination of the vertical stresses to be supported by the sill mat and the structural capacity required to withstand these loads.

In practice, sill mats are constructed based on two main approaches; experience, and engineering principles. From an engineering point of view, it has been considered beam theory or solid mechanics theory, numerical modelling, physical modelling (centrifuge modelling in some cases).[1–6] Analytical theory consider sill mats as structural elements that may fail under sliding, flexural, rotation, or caving modes of failure.[1] One of the main types of failure is the flexural failure, and the deduction of its analytical equation considers classical beam theory applied to this mining problem.[2] Further in this work is examined the applicability of this theory to this mining design.

Data of actual geometry and material properties of sill mats used in mining can be found in 3,4,6,7 and 8 and are shown in Table 1.

2. Analytical interpretation of flexure failure based on classical beam design

Vertical load (σ_v) causes the sill mat to bend, meaning that the upper surface must be shorter than the lower surface or vice versa depending of the applied load. Therefore, the strain are different along the sill mat, and because the stress is directly proportional to strain, it follows that the stress will vary through the depth of the mat. This bending creates a compressive stress in the upper portion and a traction in the lower portion of the sill mat (or vice versa depending on location). In between, there is a plane where its elements are neither stretched nor compressed, called the neutral plane. Since the constructing materials used to fabricate the sill mats have larger compressive strength than tensile strength, failure starts when the tensile stresses reach the ultimate tensile strength of the material (σ_t).

As mentioned previously, flexural failure considerations using beam theory provides the designer with a simple tool to analyze sill mat stability. In 1 is considered that “a wide sill mat would, quite obviously, be susceptible to flexural failure due to the relatively low tensile strength of cemented tailings”. He proposed the standard formulae for a fixed end uniformly loaded beam (as shown in Fig. 2).

Considering the maximum moment (M_{max}) generated at both ends (Fig. 2a), Mitchell proposed that failure occurs when the maximum traction on the sill mat (σ_{max}) reaches the maximum tensile strength (σ_t), $\sigma_t = \sigma_{max}$.

When solving the value of σ_{max}, generated by the vertical uniform

* Corresponding author.
E-mail address: cristian.caceres@uai.cl (C. Caceres).

http://dx.doi.org/10.1016/j.ijrmms.2017.09.002
Received 16 November 2016; Received in revised form 9 June 2017; Accepted 5 September 2017

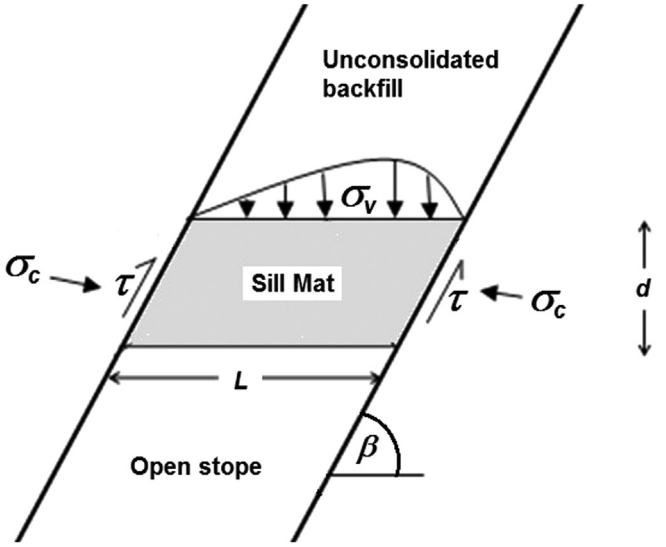

Fig. 1. Schematic representation of sill mats.

load σ_v (Figs. 1 and 2) under the adequate boundary conditions, it will be established that the geometrical condition for flexure failure will initiate at both ends of the beam, as it is shown in Fig. 2b, is given by:

$$\left(\frac{L}{d}\right)^2 > 2(\sigma_t + \sigma_c)/\sigma_v \tag{1}$$

where σ_t is the tensile strength of the sill mat and σ_v is the uniform loading which should include its self-weight. σ_c is the compressive stress applied to both ends of the beam. Thereafter, failure by traction is observed at the center of the beam as it is shown in Fig. 2c.

Eq. (1) is deduced using the Euler-Bernoulli bending theory or simple beam theory. The use of this theory involves the following hypotheses. (a) The load acting is normal to its surface. (b) Deflections are small in comparison with the thickness of the beam/plate (or Sill Mat). (c) The cross section is assumed to remain perpendicular to the axis direction. (d) The weight of the beam/plate can be included in the load σ_v. (e) Also, the problem is considered as a state of plane stress, in which the normal stress σ_z, and the shear stresses σ_{xz} and σ_{yz} are also assumed to be zero. According to the hypothesis mentioned before, the general beam equation will be deduced in the following paragraphs.

Fig. 2 shows a cross section of the beam where there is a zone in traction and the opposite side in compression. In between, there is a neutral axis, where there is no axial deformation. Considering "u_z" = w as the vertical deflection of the neutral axis, the deformation in the cross section of the beam in the x direction is given by:

$$u_x = -z\psi(x) \tag{2}$$

As the plane AB remains perpendicular to CD (Euler-Bernoulli assumption) then:

$$\psi = dw/dx \tag{3}$$

Then

$$u_x = -z\frac{dw}{dx} \tag{4}$$

and

$$\varepsilon_{xx} = \frac{\partial u_x}{\partial x} = -z\frac{d^2w}{dx^2} \tag{5}$$

Then assuming $\sigma_{yy} = \sigma_{zz} = \sigma_{xy} = \sigma_{yz} = 0$ the stress-strain relationships give

$$\varepsilon_{xx} = \frac{1}{E}[\sigma_{xx} - \nu(\sigma_{yy} + \sigma_{zz})] = \frac{1}{E}\sigma_{xx} \tag{6}$$

$$\sigma_{xx} = -Ez\frac{d^2w}{dx^2} \tag{7}$$

Then for equilibrium of momentum:

$$M = -\int_A \sigma_{xx} z dA = E\frac{d^2w}{dx^2}\int_A z^2 dA = EI\frac{d^2w}{dx^2} \tag{8}$$

$$\Rightarrow \sigma_{xx} = -Mz/I \tag{9}$$

where I is the second moment of inertia, and z is the distance from the neutral axis of the beam.

Additionally,

$$\frac{dM}{dx} = V(x),\ \frac{dV}{dx} = \sigma_z(x),\ EI\frac{d^4w}{dx^4} = \sigma_z(x) \tag{10}$$

where σ_z is the applied force/unit length on the beam in the z direction (or σ_v for this example).

Solving the above equations for the corresponding boundary conditions, the deflection w, the shear stress V, and the moment M on a beam with both ends fixed can be obtained. For this analysis the sill mat is considered with both ends fixed (as shown in Fig. 2), then it becomes a statically indeterminate beam problem. Therefore to obtain the solution for this beam the static equilibrium is used and considering known values of slope and deflection at particular beam sections, the solution for maximum moment located at both ends is given by[9]:

$$\mathrm{M_{max}} = \sigma_v L^2/12 \tag{11}$$

and the moment at the center of the beam is:

$$\mathrm{M_{max}} = \sigma_v L^2/24 \tag{12}$$

Consequently the maximum traction will be located at both ends and has a value derived from Eq. (1):

$$\sigma_{max} = \frac{M_{max} * \frac{d}{2}}{\frac{1}{12}d^3} = \frac{\frac{\sigma_v L^2}{12} \cdot \frac{d}{2}}{\frac{1}{12}d^3} = \frac{\sigma_v L^2}{2d^2} \tag{13}$$

Failure will initiate on both ends of the beam (or sill mat). Once these two points show plastic deformation, the center of the beam will start failing as shown in Fig. 2.

Considering that an additional compressive force is applied to the beam (σ_c) the maximum applied traction is: (σ_{max} - σ_c) and in order to be stable, the tensile strength σ_t has to be greater than σ_{max} - σ_c, then Eq. (1) can be deduced directly in 1.

In many simulations, the evaluation of flexure failure has been performed using this simple equation. However, in sill mat design the problem is closer to a plane strain than a plane stress approximation. This is due the fact that the longest dimension of the sill mat is much larger than the span. Additionally, the other hypothesis used to derive this equation will be discussed further after numerical model results are shown. More details about Euler-Bernoulli beam theory can be found in 9–11.

3. Numerical modelling approach for sill mats

FLAC 2D version 7 was the numerical modelling code employed for modelling and estimating the factor of safety of different sill mat geometries under varying strength properties. FLAC uses a finite difference approach that allows the use of different constitutive models to represent rock mass or any other material as a continuum in order to determine its behavior under the loads being applied. Fig. 3 shows the mesh used in the numerical model. The dimensions of the elements of the mesh is maintained constant independently of the size of the modelled sill mat. The unit weight of the backfill material was imposed at very low value since the vertical load σ_v takes into consideration the self-weight of the sill mat.

Only flexure resistance of the sill mat (tensile failure) will be considered in this analysis. Therefore, shear strength will be imposed at

Table 1
Underhand cut and fill database (from Pakalnis 7).

	MINE	%CEMENT	*L* SPAN (m)	*d* SILL THICKNESS (m)	UCS (MPa)	COMMENTS	REASON FOR MINING UNDER SILL MAT
1	RED LAKE MINE	10	6.1	3 (~ 0.6 m air gap)	1.5	PASTE DESIGN STRENGHT GOVERN TIME TO MINE UNDER (14 day − 28 day)	STRESS ~2000 m DEPTH
2a	ANGLOGOLD (1999 VISIT)	6.5	7.6	4.6	5.5	CRF	WEAK RMR ~ 25 +
2b	MURRAY MINE	8	9.1	4.6	6.9	CRF DESIGN	
2c	QUEENSTAKE-2004	8	21	4.6	6.9	MINED REMOTE - NO CAVE 2" MINUS AGGREGATE GO UNDER A MINIMUM OF 14days, WALL CRF 5–6% BINDER JAM TIGHT TO BACK/STEEP	
3	ESKAY	7	3	3	4–12	CRF (4 MPa DESIGN) UCS is 11 MPa (28 day)	WEAK RMR ~ 25 +
4a	TURQUOISE RIDGE	9	13.7	4	8.3	CRF TEST PANEL	
4b		9	3.7	3	8.3	CRF DRIFT & FILL	WEAK RMR ~ 25 +
4c		9	7.3	3	8.3	CRF PANEL	
5	MIDAS	7	2.7	3	3.4	CRF	WEAK RMR ~ 25 +
6	DEEP POST	6.75	4.9	4.3	4.8	CRF GO UNDER IN 28days	WEAK RMR ~ 25 +
					0.7	PASTE (FS = 1.5)	
7a	STILLWATER - NYE	10	1.8	2.7	0.3	GO UNDER IN 7days–28days	
7b			2.4	2.7	0.5	5% BINDER - 0.5 MPa UCS 28days	
7c			3	2.7	0.7	7% BINDER - 0.7 MPa UCS 28days	STRESS ~ 800 m DEPTH
7d			3.7	2.7	1	10% BINDER - 1.0 MPa UCS 28days	
7e			4.3	2.7	1.4	12% BINDER - 1.2 MPa UCS 28days	
7 f			4.9	2.7	1.8		
7 g			5.5	2.7	2.3		
7 h			6.1	2.7	2.9		
8	MIEKLE SOUTH (BARRICK)	7	4.6–6.1	4.6	5.5	CRF	WEAK RMR ~ 25 +
9	GOLD FIELDS - AU	10	5	5	4.5	CRF	WEAK RMR ~ 25 +
10	STRATORI MINE (TVX)	12.8	6.0–9.0	6	2	HIGH DENSITY SLURRY (78% WEIGHT SOLIDS)	WEAK RMR ~ 25 +
11	GALENA (COEUR DE ALENE)	10	3	3 (~ 0.9 m air gap)	2.5	10% CEMENTED HYDRAULIC FILL (73–75% WEIGHT SOLIDS) (UCS after 7days)	STRESS ~ 1000 m DEPTH
12	LUCKY FRIDAY - HECLA (GOLD HUNTER)	8	2.4–4.6	3 (~ 0.6 m air gap)	4.8	GO UNDER IN 3days (2.4 MPa UCS) 8% PASTE (COARSE TAILS) (No free water)	STRESS ~ 2000 m DEPTH
13	KENCANA MINE (NEWCREST)	12–24 vs dry tuff	6.0–8.0	5	1.2–1.5	1.2 MPa IN BACK AND 0.5 MPa IN WALLS DESIGN STRENGTH GOVERN TIME TO GO UNDER PASTE 7days − 28days	WEAK RMR ~ 25 +
14	LANFRANCHI NICKEL MINES (HELMUTH SOUTH)	4.0–8.0	6.0–12.0* *INTERS	5	1.2–2.0	SPAN 6 m UNDER PASTE SPAN 12 m INTERSECTIONS CABLED (6 m) TO GO UNDER PASTE 14days	STRESS ~ 850 m DEPTH
15	CORTEZ HILLS (BARRICK)	7.8	6.0–11.0* *INTERS	4.6	6	GO UNDER IN 28days SPAN IS 6 m WITH 11 m AT INTERSECTIONS MAXIMUM TOP SIZE 5 cm (2")	WEAK RMR ~ 15 +
16	ANDAYCHAGUA MINE (VOLCAN)	14	5.0–15.0	3.5	16 +	CEMENTED AGGREGATE FILL SPAN IS 15 m AGGREGATE FILL − 3/4"	WEAK RMR ~ 15 +

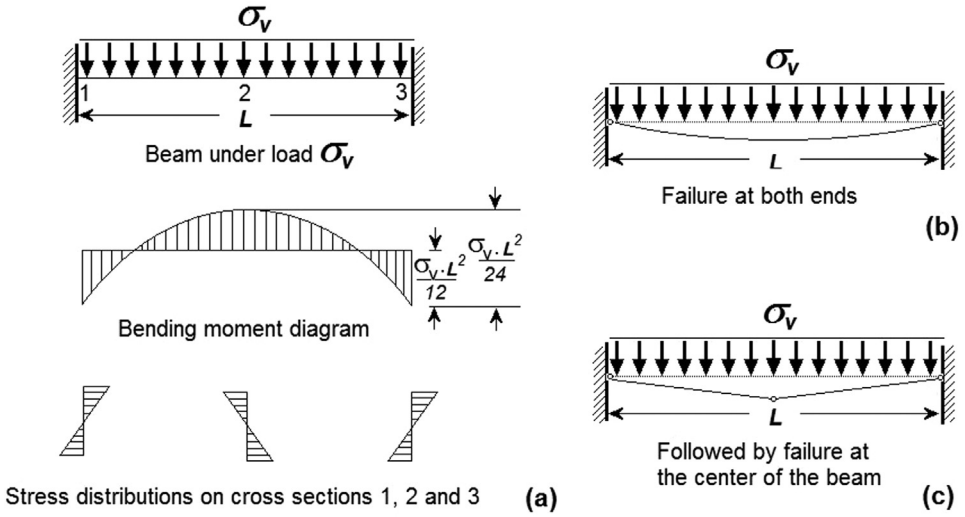

Fig. 2. Yielding points according to classical beam theory.

much higher values than the expected strength of actual Sill Mat material, using Mohr-Coulomb model with high values of cohesion (c = 60 MPa) and friction angle (ϕ = 38°), to avoid shear failure. Therefore, tensile resistance (σ_t) is considered as the main strength parameter in the model, as in the analytical model explained previously. Consequently, only the flexure failure mode is compared using the analytical and numerical modelling results. In both cases the onset of failure is achieved when the traction on layers of the sill mat exceeds the tensile strength of the material (σ_t), which is reduced in the numerical model until failure is reached.

Multiple sill mat geometries are evaluated considering different aspect ratios L/d (see Table 2). Vertical load σ_v applied to the top layer of the sill mat is assumed constant and equally distributed along the top surface of the sill mat and is set at 1.0 MPa. Other studies previously carried out have estimated this load (σ_v) as it is shown in 3,4, so the applied load is in the expected range. Even though this work uses a constant vertical load σ_v, the conclusions obtained are still valid for other loads, as the maximum tension on the sill mat will increase proportionally to σ_v in the analytical and numerical model. A value of $\sigma_{tBeam}/\sigma_{tNM}$ = 100.00 is assumed when failure is not reached

4. Results and discussion on the validity of the use of classical flexure failure equations on sill mat design

Numerical models are performed to compare its results with the corresponding analytical equation previously shown. The comparison is performed in terms of the required tensile strength (σ_t) using both methods.

Therefore for a given geometry, the minimum σ_t derived using the classical beam equation[1] that defines the onset of flexural failure on the sill mat is σ_{tBeam}. On the other hand, the same geometry is numerically modelled using the approach previously explained. The tensile strength of the material is initially specified at a higher value than the value obtained by Mitchell's equation. In the numerical model for a given L/d ratio if the imposed tensile strength does not cause flexural failure, then the tensile strength σ_t is decreased until failure is achieved. The onset of σ_t at failure by flexure using the numerical modelling procedure is defined as σ_{tNM}. This approach is repeated for different L/d ratios. The results of the ratio $\sigma_{tBeam}/\sigma_{tNM}$ for all combinations shown in Table 2 is shown in Fig. 4, for a Poisson's ratio of 0.3 being a reasonable value for sill mat materials.

Fig. 4 shows that the ratio $\sigma_{tBeam}/\sigma_{tNM}$ are closed to 1.0 when the ratio L/d is larger than 8.5, even though these values start to increase slightly for larger values of L/d. Also, it can be observed that for L/d ratios lower than 8.5 the σ_t value obtained analytically at the onset of failure is higher than the value obtained by numerical modelling. This means that for values of L/d smaller than 8.5, Mitchell's equation is considerably more conservative than the numerical modelling results, as the σ_t values to maintain sill mat stability are larger.

These results complement the conclusion obtained previously by 1, where for values of L/d between 2.33 and 2.63 (see Fig. 4) centrifuge models also showed no failure by flexure even though analytical

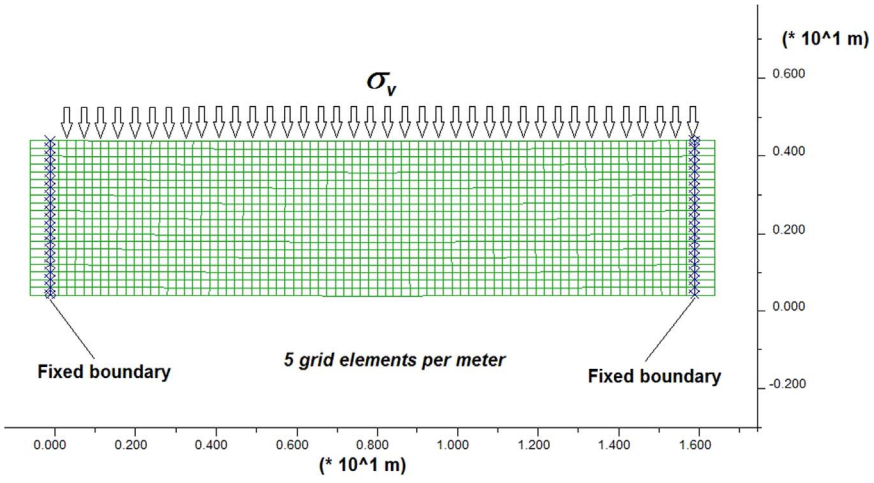

Fig. 3. Modelling mesh showing elements, fixed boundaries and loads (five grid elements per meter).

Table 2
Comparison of modelling (σ_{tNM}) and analytical (σ_{tBeam}) tensile strength results.

Length L (m)	Height d (m)	Aspect Ratio L/d	σ_c (MPa)	σ_{tNM} (MPa)	σ_{tBeam} (MPa)	Ratio $\sigma_{tBeam}/\sigma_{tNM}$ ()
20.0	4.50	4.4	4.53	0.0	5.3	100.00
20.0	4.00	5.0	5.75	0.0	6.8	100.00
20.0	3.00	6.7	10.77	0.0	11.5	100.00
40.0	5.75	7.0	9.53	1.0	14.7	14.67
20.0	2.50	8.0	14.78	1.0	17.2	17.22
39.0	4.75	8.2	17.93	2.0	15.8	7.89
29.0	3.50	8.3	16.18	2.5	18.1	7.26
27.0	3.25	8.3	16.70	3.0	17.8	5.94
25.0	3.00	8.3	17.25	4.0	17.5	4.37
23.0	2.75	8.4	15.62	10.0	19.4	1.94
21.0	2.50	8.4	16.00	9.0	19.3	2.14
17.0	2.00	8.5	15.92	14.0	20.2	1.44
30.0	3.50	8.6	2.60	29.0	34.1	1.18
40.0	4.50	8.9	10.40	33.0	29.1	0.88
29.0	3.00	9.7	2.45	38.0	44.3	1.17
40.0	4.00	10.0	1.08	48.0	48.9	1.02
20.0	2.00	10.0	5.19	33.0	44.8	1.36
25.0	2.50	10.0	3.39	33.0	46.6	1.41
32.0	3.00	10.7	1.44	51.0	55.4	1.09
33.0	3.00	11.0	1.07	53.0	59.4	1.12
32.0	2.75	11.6	0.56	54.0	67.1	1.24
36.0	3.00	12.0	0.56	56.0	71.4	1.28
28.0	2.25	12.4	0.29	55.0	77.1	1.40
26.0	2.00	13.0	1.02	55.0	83.5	1.52
28.0	2.00	14.0	3.65	59.0	94.4	1.60
30.0	2.00	15.0	6.66	60.0	105.8	1.76
40.0	2.50	16.0	11.67	66.0	116.3	1.76
36.0	2.00	18.0	19.30	64.0	142.7	2.23
40.0	2.00	20.0	26.33	67.0	173.7	2.59

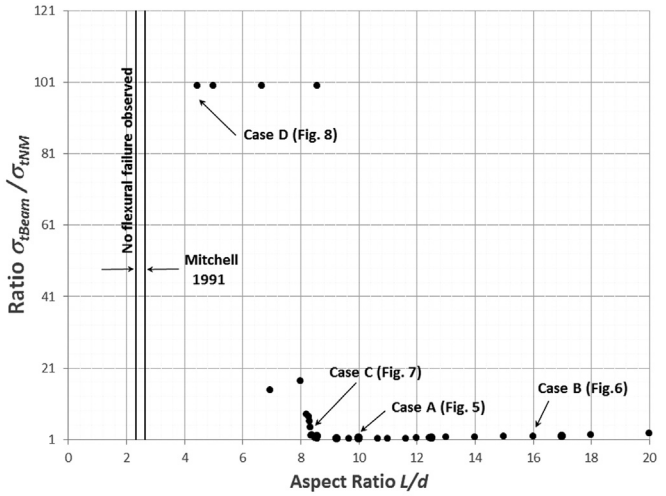

Fig. 4. Ratio of deduced sill mat using beam theory and numerical modelling (Poisson's ratio = 0.3).

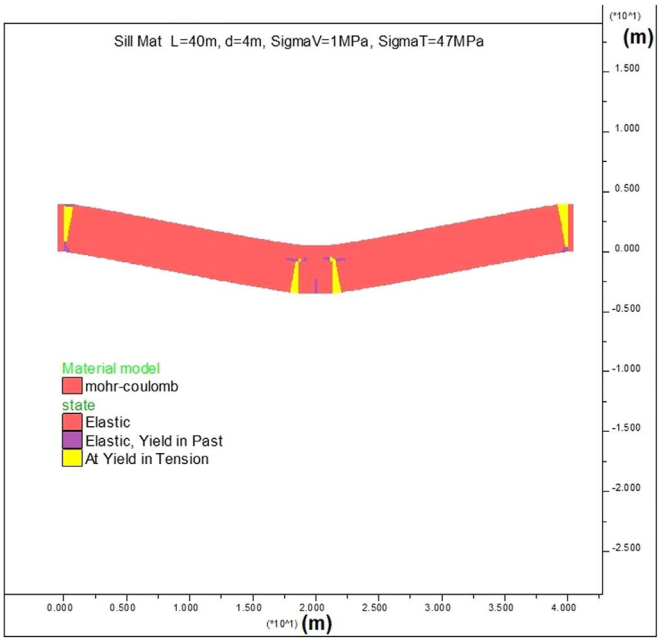

Fig. 5. Case A Aspect ratio L/d = 10.

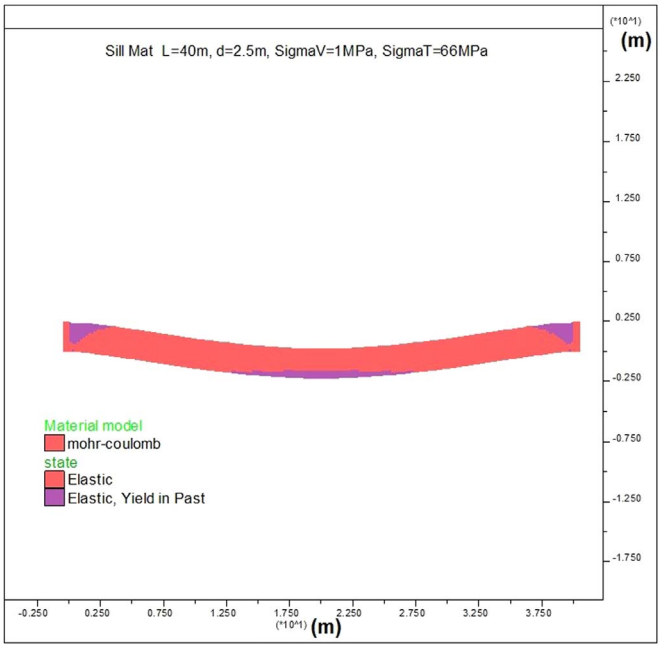

Fig. 6. Case B Aspect ratio L/d = 16.

predictions forecast failure.

Modelling results are shown for four different cases as the one depicted in Fig. 5. Fig. 5 shows the result for case A when the ratio L/d is equal to 10.0, and Fig. 6 shows the case when the ratio L/d is equal to 16.0 (Case B). It can be observed from the numerical modelling that in both cases (A and B), the failure mechanism is very close to the classical theoretical flexure failure in beams (Fig. 2). First, two tensile failure zones are developed at both ends of the sill mat followed by a third point of failure observed at the center of the beam (second maximum moment).

As values of L/d become larger, the deflection of the sill mat is larger. Therefore, for large L/d ratios (> 12.0), the hypothesis of small deflections used for deriving the flexural failure analytical equation is not completely correct.

Case C shows the results for a sill mat with $L/d = 8.5$ ratio (Fig. 7). It can be observed that flexural failure still develops, however boundary forces start becoming very important in the solution and therefore influences the maximum tensile loads on the sill mat.

Case D shows the results of numerical model for $L/d = 5$ (Fig. 8), where it was not possible to attain flexural failure even for zero values of σ_t. In this case, boundary conditions affects not only the boundaries of the sill mat but all the structure. This type of load concentrations has been explained using St. Venant´s principle. Previous work has shown difficulties to predict stresses in the boundary zone as it is shown in 12–14.

Figs. 9 and 10 shows the horizontal stresses in cases C and D. In the case of short sill mats (case D) the applied vertical stress generates

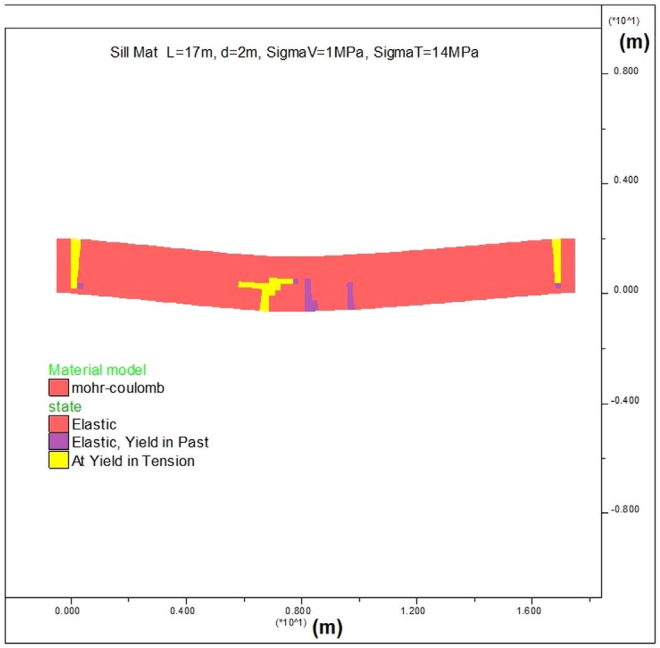

Fig. 7. Case C aspect ratio L/d = 8.5.

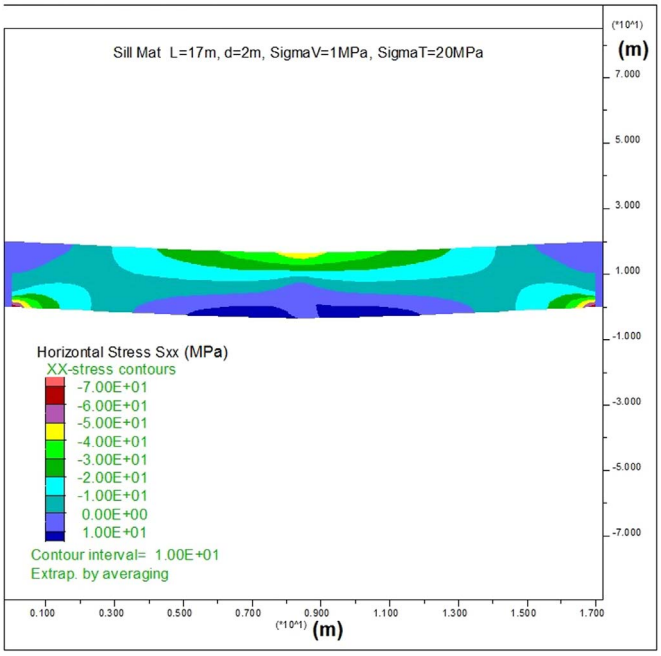

Fig. 9. Case C – horizontal stress σ_{xx} (MPa) for aspect ratio L/d =8.5.

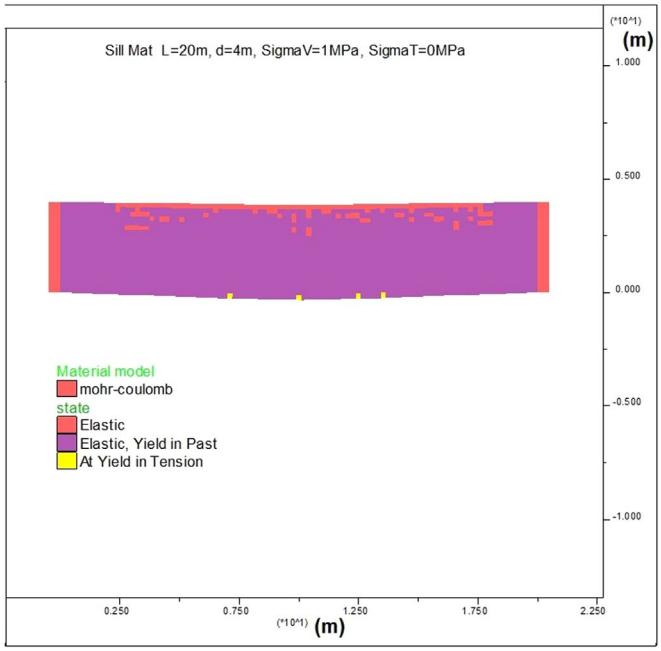

Fig. 8. Case D aspect ratio L/d = 5.

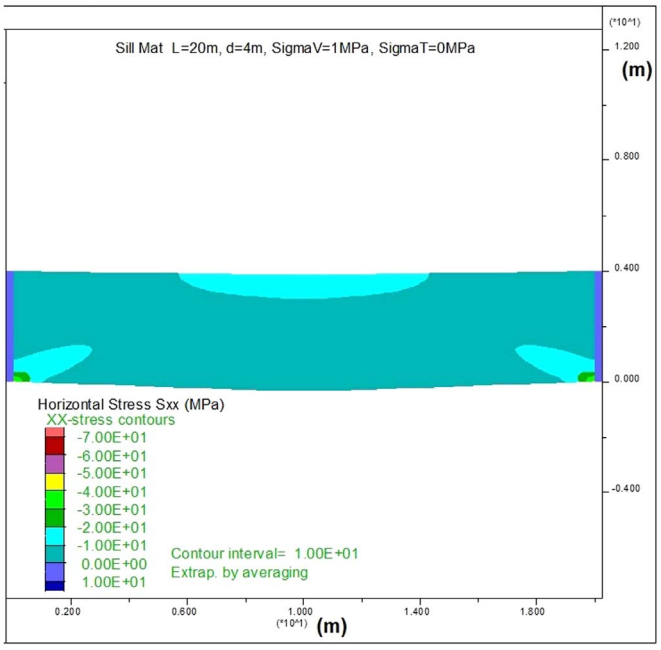

Fig. 10. Case D – horizontal stress σ_{xx} ((MPa) for aspect ratio L/d =5.

horizontal stresses that decrease the expected traction due to flexion in the ends of the sill mat. This implies that flexural failure is not generated in case D.

Fig. 11 shows a comparison of the $\sigma_{tBeam}/\sigma_{tNM}$ ratio for three different values of the Poisson's ratio: 0.3, 0.4999 and 0.0001. It is observed from this figure that even though there are some changes in the ratio between analytical and numerical values necessary to trigger failure by flexure, the general trend commented previously is maintained independent of the Poisson ratio used in the numerical model.

Therefore, from the numerical modelling results obtained, it is possible to assume that for boundary conditions considered in flexure failure, that is fixed at both ends of the sill mat, it is not possible to obtain failure for ratios of L/d lower than 6.7. Using Mitchell's flexural equation for beams with both ends fixed will result in a very conservative approach for values of L/d between 6.7 and 8.5. On the other hand, Mitchell's equation will only produce slightly conservative results for values of L/d between 8.5 and 20.0 and consequently it could be used for design according to the results shown in this work. For larger values of L/d the deflection of the sill mat is significant and so Mitchell's equation starts to yield more conservative results as it assumes small deformations.

Additionally, when the historical sill mat data (from 4 and 7) is compared against the modelling results, it is observed that actual sill mat geometries are within a range where the traditional flexure equation is too conservative, or flexure failure does not developed at all (Fig. 12) or at the most, its use is too conservative.

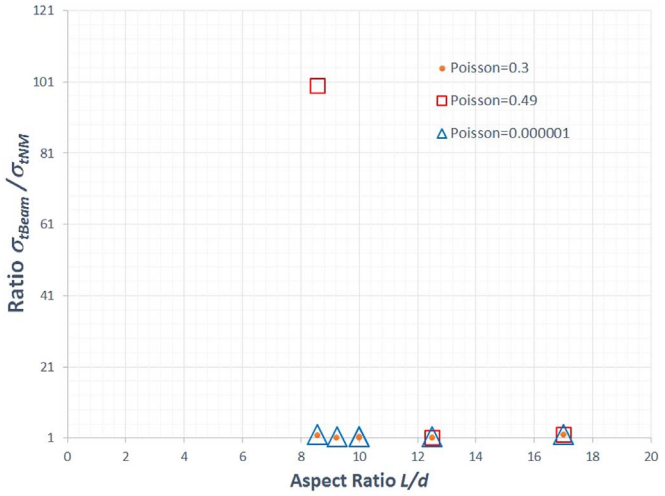

Fig. 11. Influence of Poisson's ratio with respect to the $\sigma_{tBeam}/\sigma_{tNM}$ ratio.

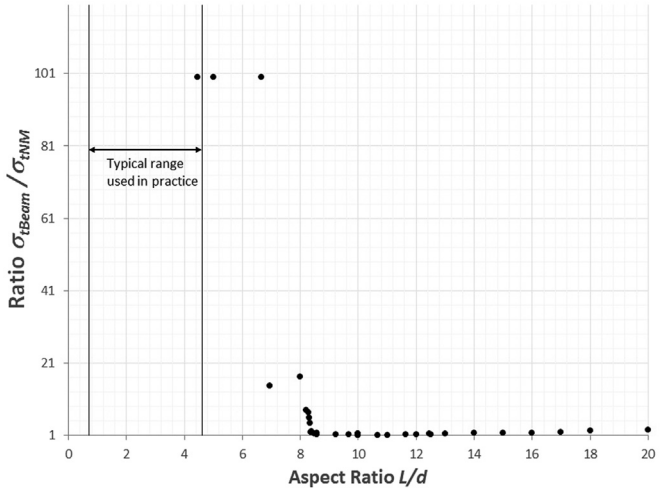

Fig. 12. Typical range of existing sill mats compared to flexural failure (Poisson's ratio = 0.3).

5. Conclusions

In this work was analyzed the range of validity of Mitchell's flexure failure equation for sill mats considering both ends fixed. The validity of Mitchell's equation was established using numerical modelling results. The following conclusions are based on the results of numerical models involving different geometries for sill mats.

These results showed that flexure failure will unlikely develop for ratios of L/d lower than 6.7. The use of analytical formulae to obtain the factor of safety of a sill mat in this range is highly conservative. Saint Venant´s principle explain the fact that no failure by flexure is obtained for values of $L/d < 6.7$. Higher horizontal stresses are observed in these cases as the boundary effect is strong in these cases.

Sill mats with values of L/d between 6.7 and 8.5 will yield conservative results. These will be more conservative as the value of L/d is closer to 6.7. On the other hand, Mitchell's equation will produce slightly conservative results for values of L/d between 8.5 and 20.0 and consequently it could be used for sill mat design according to the results shown in this work. For larger values of L/d, that is greater than 12, the deflection of the sill mat is significant and thus Mitchell's equation yields conservative results as it assumes the hypothesis of small deformations. Most of the actual geometries from mines fall in the zone where no failure by flexure is expected. The Mitchell equation must be used considering this fact.

References

1. Mitchell RJ. Sill mat evaluation using centrifuge models. *J Min Sci Technol.* 1991;13:301–313.
2. Caceres C, Pakalnis R, Hughes P, Brady T. Numerical modeling approach of failure modes for cemented backfill sill mats. In: *Proceedings of American Rock Mechanics Association*; 2007:ARMA-07-195.
3. Marcinyshyn KW. *Sill Mat Design for Narrow Vein Mining [M.Sc. thesis].* British Columbia: The University of British Columbia; 1996.
4. Pakalnis R, Caceres C, Clapp K, Morin M. Design spans- Underground cut and fill mining. In: *Proceedings of the 107th CIM-AGM*. Toronto; April. 2005:1–9.
5. Tesarik DR, Seymour JB, Yanske TR. Long-term stability of a backfilled room-and-pillar test section at the Buick Mine, Missouri, USA. *Int J Rock Mech Min Sci.* 2009;46(7):1182–1196.
6. Caceres C. *Effect of Backfill on Open Stope Mining Methods [MASc thesis].* British Columbia: Mining Engineering, University of British Columbia; 2005.
7. Pakalnis R. Empirical design methods in practice. In: *Proceedings of the International Seminar on Design Methods in Underground Mining.* Perth; November 2015:37–56.
8. Hughes PB, Pakalnis R, Deen J, Ferster M. Cemented paste backfill at stillwater mine. american rock mechanics association. In: *Proceedings of the 47th U.S. Rock Mechanics Symposium.* San Francisco; June 2013:23–26.
9. Megson THG. *Structural and Stress Analysis.* Amsterdam: Elsevier; 2005.
10. Beck AT, da Silva Jr CRA. Timoshenko versus Euler Beam Theory: pitfalls of a deterministic approach. *Struct Saf.* 2011;33:19–25.
11. Carrera E, Giunta G, Petrolo M. *Beam Structures: Classical and Advanced Theories.* New York: Wiley; 2011.
12. Lee K-H, Goel SC, Stojadinovic AB. Boundary effects in steel moment connections. In: *Proceedings of the 12 WCEE Conference*. Auckland; January. 2000:1098–1106.
13. Ahmed SR, Khan MR, Islam KMS, Uddin Md.W. Investigation of stresses at the fixed end of deep cantilever beams. *Comput Struct.* 1998;69:329–338.
14. Asghari M, Kahrobaiyan MH, Rahaeifard M, Ahmadia MT. Investigation of the size effects in Timoshenko beams based on the couple stress theory. *Arch Appl Mech.* 2011;81:863–874.